Catalysis Science & Technology

ROYAL SOCIETY OF CHEMISTRY

PAPER

View Article Online
View Journal | View Issue

Cite this: *Catal. Sci. Technol.*, 2026, **16**, 3280

Thermally treated polyvinyl chloride (PVC)-derived highly microporous carbon support: applications in hydrotreating catalysis

Ju Young Kim,†[ab] Seung Gun Kim,†[c] Jisong Kang,[ab] Jae-Wook Choi,[a] Chun-Jae Yoo,[adef] Chang Soo Kim,[ad] Kyeongsu Kim,[ad] Seongmin Jin,[ad] Hyunjoo Lee,[adg] Kwang Ho Song,[b] Jungkyu Choi,[b] Dalsu Choi *[c] and Jeong-Myeong Ha *[ad]

Received 31st December 2025,
Accepted 20th March 2026

DOI: 10.1039/d5cy01613d

rsc.li/catalysis

Chemical recycling of polyvinyl chloride (PVC) *via* depolymerization is more challenging than that of polyolefins because hydrogen chloride forms during thermal degradation. The thermal degradation of PVC yields a solid residue after dehydrochlorination, which, upon KOH treatment at 800 °C, produces a highly microporous carbon material with a maximum BET surface area of 3273 m^2 g^{-1}. A ruthenium catalyst supported on this PVC-derived carbon exhibits high catalytic activity for the hydrodeoxygenation of guaiacol. The highly microporous carbon support prepared in this study serves as a valuable upcycled product for various applications.

1. Introduction

High-surface-area carbon materials attract considerable interest because of their applications in separation,[1] catalysis,[2] electrochemistry,[3] and other chemical processes. Carbon materials are obtained by the carbonization of biomass, coal, petroleum, and polymers, and plastic wastes represent a promising candidate for producing carbon materials *via* their upcycling process.

The global regulations for suppressing environmental hazards and global warming demand the recycling of plastic wastes.[4] To address these issues, the conversion of plastic wastes to recycled polymers and valuable upcycled products has been proposed as a viable strategy. Among plastics, polyvinyl chloride (PVC), which is produced and consumed in increasing amounts, raises environmental concerns because the chlorine in PVC remains hazardous throughout its life cycle.[5–7] For example, the landfill disposal of PVC causes toxic gas emissions or long-term pollution. Recycling of PVC has been attempted *via* physical or chemical routes, including melting followed by compounding,[8] solvent extraction,[9] and thermolysis processes such as pyrolysis and gasification,[10] along with the dechlorination.[11] While recycling processes exist for PVC wastes, environmentally benign recycling remains difficult because their high chlorine content generates corrosive hydrogen chloride (HCl) during thermal processing, and this necessitates the conversion of PVC into non-PVC materials before recycling.[12–15] A substantial amount of char with limited practical value is also formed during the thermolysis of PVC.[12,16]

Previous studies on PVC recycling primarily focus on the efficient removal of HCl and the production of value-added products through various approaches, including the co-pyrolysis of PVC with biomass,[17–19] hydrothermal treatments,[20–23] the use of alkaline additives such as NaOH and KOH,[24] and catalytic pyrolysis.[12,25,26] These approaches primarily emphasize environmental benefits and the production of high-value chemicals. However, considering the practical utilization of PVC wastes, thermal degradation is an inevitable step, and the effective use of the resulting carbonaceous char is essential to achieve a more complete and realistic recycling strategy.

While the pyrolysis of plastic wastes is frequently used to chemically depolymerise plastics and regenerate their monomers, the thermolysis of PVC produces paraffins, olefins, and aromatics as gas or liquid products, along with the carbon-like char.[12] The hydrocarbon products can be used as petrochemical feedstocks, including fuel and

[a] *Clean Energy Research Center, Korea Institute of Science and Technology, Seoul 02792, Republic of Korea. E-mail: jmha@kist.re.kr*
[b] *Department of Chemical and Biological Engineering, Korea University, Seoul 02841, Republic of Korea*
[c] *Department of Chemical Engineering, Myongji University, Yongin, Gyeonggi-do 17058, Republic of Korea. E-mail: dalsuchoi@mju.ac.kr*
[d] *Division of Energy and Environment Technology, KIST School, University of Science and Technology, Seoul 02792, Republic of Korea*
[e] *School of Chemical Engineering, Sungkyunkwan University, Suwon 16419, Republic of Korea*
[f] *KIST-SKKU Carbon-Neutral Research Center, Sungkyunkwan University, Suwon 16419, Republic of Korea*
[g] *KU-KIST Graduate School of Converging Science and Technology, Korea University, Seoul 02841, Republic of Korea*
† These authors contributed equally.

naphtha, but the solid waste possesses limited value for further applications.

In this study, high-surface-area carbon materials are prepared *via* the thermolysis of PVC for their application as a catalyst support. The elimination of HCl and the change in the solid residue structure are controlled by altering the thermolysis temperature,[13,27] and the residue structure exhibits limited porosity and a low surface area when carbonization occurs at low temperatures (<400 °C). Subsequent chemical activation using potassium hydroxide (KOH) generates highly porous structures.[17,28,29] The type of solid residue obtained *via* the thermal decomposition of PVC is adjusted by controlling the reaction temperature. The performance of the resulting activated carbons is evaluated and compared with that of commercially available carbon supports to assess their potential for practical applications and valuable utilization. The hydrodeoxygenation (HDO) of guaiacol, a lignin-derived phenolic compound, is performed to measure the catalytic activity of the carbon-supported metal catalysts. Guaiacol is selected as the lignin-derived model compound because its HDO reaction depends strongly on the properties of carbon supports. This reaction therefore provides a suitable probe to examine whether the PVC-derived carbon materials function as effective supports for Ru catalysts in HDO reactions.

2. Methods

2.1 Materials

PVC (product number: 346764), 4-ethylguaiacol ($C_9H_{12}O_2$; ≥98%), activated carbon, and ruthenium(III) chloride ($RuCl_3$; 99.9%) were purchased from Sigma-Aldrich (Milwaukee, Wisconsin, USA). The chloride content in PVC was 56.77%, and the molecular weight was approximately 233 000 g mol^{-1}. Carbon black was purchased from Alfa Aesar (Ward Hill, Massachusetts, USA). KOH flakes (Daejung Chemicals & Metals, Anseong, Republic of Korea) were used for chemical activation. A hydrogen/argon gas mixture (5% (v/v) H_2 in Ar) and nitrogen gas (N_2, 99.999%) were purchased from Sinyang Medicine (Anseong, Republic of Korea). Deionized (DI) water was prepared using a water purification system (AquaMax Ultra 370, YoungIn Chromass, Anyang, Republic of Korea).

2.2 Thermal treatment of PVC

PVC was heated using a three-neck flask *via* a semi-batch process.[12] PVC powder (10 g) was placed in the reactor. Before the reaction, N_2 gas was purged through the system at a flow rate of 100 mL min^{-1} for 1 h. After purging, the reactor was stirred at 110 °C for 20 min under a continuous N_2 flow (100 mL min^{-1}) to remove moisture from the reactant and the reactor. Along with N_2 flow, the reactor was heated to the target temperature (200, 250, 300, 350, or 450 °C), and this temperature was maintained for 1 h. The vapor from PVC was condensed at two cold traps (70 °C and 0 °C). The gas mixture was washed using a water trap to remove HCl. The thermally degraded PVC solid residue was denoted as R-*X*, where *X* is the reaction temperature.

2.3 Preparation of the KOH-treated PVC solid residue

One-step activation was conducted using a tube furnace (SH Scientific, Sejong, Republic of Korea) (Fig. S1). A mixture of 1 g of PVC residue (R-250 and R-350) and 4 g of KOH flakes was placed in an alumina crucible. Before activation, N_2 was purged through the system at a flow rate of 150 mL min^{-1} for 1 h. After purging, the furnace was heated to 800 °C at a ramping rate of 5 °C min^{-1} under a continuous N_2 flow, and this temperature was maintained for 1 h. The activated product was washed with DI water until the pH of the filtrate reached 7. Two-step activation was performed under identical furnace conditions (Fig. S1). Before chemical activation, the sample (R-250 or R350) was heated to 800 °C at a rate of 5 °C min^{-1} and held for 10 min under the N_2 flow for carbonization. Chemical activation followed the same procedure as that used in the one-step activation. The PVC solid residue treated with KOH is denoted as K-*X*, where *X* indicates the temperature of the PVC thermolysis (250 °C or 350 °C).

2.4 Preparation of the catalysts

Carbon-supported Ru (Ru/C) catalysts were prepared using the wet impregnation method. Activated carbon, carbon black, K-250, and K-350 were used as catalyst supports. The Ru loadings were 0.849 wt% for carbon black, 1.12 wt% for activated carbon, 1.29 wt% for K-250, and 0.930 wt% for K-350, as confirmed by inductively coupled plasma optical emission spectrometry (ICP-OES; iCAP 6000 Series, Thermo Fisher Scientific). Ruthenium(III) chloride (99.9%) was dissolved in DI water (15 mL) in a 250 mL round-bottom flask and stirred for 15 min at room temperature. The four types of supports were added to the Ru solution and stirred for 1.5 h. The mixture was subjected to solvent evaporation using a rotary evaporator at 50 °C. The material was dried at 105 °C in air for 16 h to remove remaining moisture. Reduction was performed under a flowing 5% H_2/Ar gas flow at 60 mL min^{-1} at 300 °C for 4 h.

2.5 Characterization of the catalysts

Pore structures and surface areas were observed *via* N_2 physisorption using a Micromeritics ASAP 2020 gas adsorption analyzer. The BET surface area (S_{BET}) was calculated based on the Brunauer–Emmett–Teller (BET) model, and the pore size distribution was calculated using the Barrett–Joyner–Halenda (BJH) method. External and micropore surface areas were calculated through *t*-plot analysis. The thermal decomposition of PVC and coke formation on the spent catalysts were quantified *via* thermogravimetry (TG) analysis using a SDT Q600 analyzer (TA Instruments). For coke quantification, the spent catalyst samples (10–20 mg) were heated to 50 °C for 10 min under an N_2 flow (100 mL min^{-1}) and heated further to 900 °C at a

Table 1 Yields and elemental compositions of the PVC reactant and its thermally treated products

Compound	Yield of thermal treatment[a] (wt%)		Elemental content in the solid residue[b] (wt%)			H/C (mol mol^{-1})	(H + Cl)/C (mol mol^{-1})
	Solid	Gas	C	H	Cl[c]		
Raw PVC	n.a.	n.a.	38.6	4.9	56.5	1.5	2.0
R-200	39.4	60.6	68.1	6.0	25.9	1.1	1.2
R-250	38.8	61.2	78.9	6.7	14.4	1.0	1.1
R-300	34.9	65.1	91.0	7.4	1.6	0.97	0.98
R-350	21.3	78.7	92.2	7.4	0.4	0.96	0.96
R-450	7.4	92.6	94.1	3.8	2.1	0.48	0.49

[a] Calculated *via* mass balance: solid + gas = 100%. A negligible yield of liquid products was observed. [b] Calculated through elemental analysis. [c] Calculated by difference from elemental analysis: Cl (wt%) = 100 − C (wt%) − H (wt%).

heating rate of 10 °C min^{-1} under air flow (100 mL min^{-1}). X-ray diffraction (XRD) results were obtained using a Rigaku D/MAX-2500V/PC equipped with an RINT2000 vertical goniometer. Cu Kα_{ave} radiation (λ = 0.15418 nm) served as the X-ray source, and XRD was performed at 40 kV and 100 mA. Particle distributions on the carbon-supported catalysts were examined *via* high-angle annular dark-field scanning transmission electron microscopy (HAADF-STEM) using Talos F200X (FEI).

2.6 Hydrotreating of guaiacol

The HDO reaction was performed in a 150 mL batch reactor. Before the reaction, the system was purged three times with N_2 to eliminate residual gases. The reaction was performed under an H_2 atmosphere (10 bar) at 250 °C for 2 h. Guaiacol (1 g), a frequently used lignin-derived phenolic compound, was used as the reactant. The reactant was dissolved in 30 mL of *n*-decane, which served as the solvent, and mixed with 10 mg of solid catalysts. Ru/C catalysts were used, each supported on a different carbon material, to investigate the influence of the support.

2.7 Characterization of the reactants and products

The elemental compositions of the reaction products were analyzed using an elemental analyzer (Flash 2000, Thermo Fisher Scientific). Liquid-phase products were identified *via* gas chromatography-mass spectrometry (GC-MS; 5975C MSD, Agilent Technologies) equipped with an HP-5MS capillary column (60 m × 0.25 μm × 0.25 mm). Liquid-phase products were quantified using gas chromatography with a flame ionization detector (GC-FID; 7890B, Agilent Technologies) equipped with an HP-5 capillary column (60 m × 0.25 μm × 0.25 mm). Solid-state NMR measurements were performed using a Bruker AVANCE III HD 400 MHz spectrometer (WS004, Korea Basic Science Institute, Metropolitan Seoul Center) equipped with a 4.0 mm magic-angle spinning (MAS) probe. The chlorine content of the solid products was analysed through combustion ion chromatography (CIC) using an ICS-2100 instrument (Thermo Fisher Scientific) equipped with an automatic combustion furnace (AQF-2100H) and a gas adsorption unit (GA-211, Mitsubishi Chemical Group). Samples were combusted at 950–1050 °C for 20 min.

3. Results and discussion

3.1 Structures of the solid residue depending on the thermolysis temperature

The removal of chlorine *via* the thermal treatment of PVC was performed (Table 1 and Fig. 1). At 200–350 °C, the H/C ratio reaches 0.96–1.1 mol mol^{-1} from 1.5 mol mol^{-1} for raw PVC, which suggests that dehydrochlorination and dehydrogenation produce polyene intermediates.[12] At 450 °C, the H/C ratio decreased to 0.48 mol mol^{-1}, which indicates carbon or char formation. The remaining H or Cl fractions ((H + Cl)/C = 0.49 mol mol^{-1}) suggest the formation of less carbonized solids. The decrease in the H/C and (H + Cl)/C ratios indicates that dehydrochlorination and dehydrogenation processes involve radical generation. The yield of the solid residue decreases from 39.4 wt% at 200 °C to 7.4 wt% at 450 °C as the temperature increases.

Changes in the polymer structure during the thermal degradation of PVC are confirmed using ^{13}C NMR spectra (Fig. 2). The alkyl peaks (sp^3) at 20–50 ppm, observed at 200–

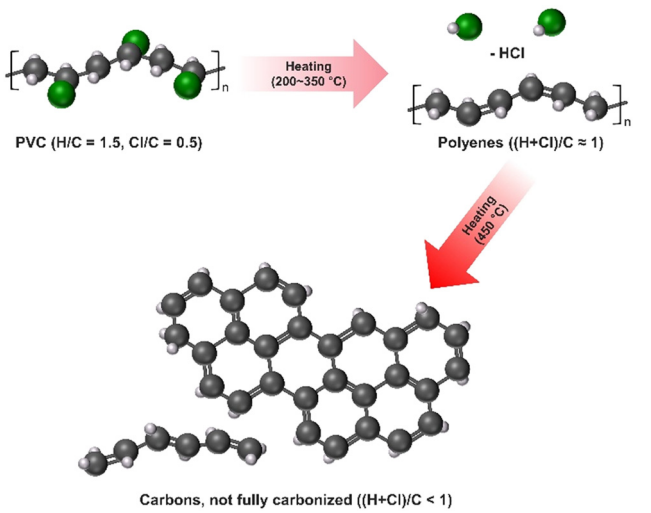

Fig. 1 Thermal degradation of PVC.

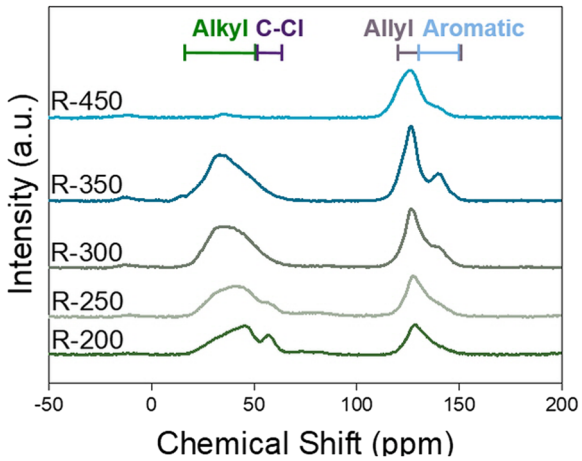

Fig. 2 ^{13}C NMR results of the thermally treated PVC solid residues.

350 °C, disappear at 450 °C, which indicates the removal of C–C bonds *via* heating. C–Cl peaks, observed at 200–250 °C, disappear at 300–450 °C, which confirms the Cl removal observed in the elemental analysis (Table 1). Allyl peaks (sp^2, 120–150 ppm) are observed at 200–450 °C, and the formation of aromatic carbons (sp^2, 130–150 ppm) is identified at 250–300 °C. These observations indicate that both allyl and aromatic carbons coexist. The formation of alkynyl bonds (sp, 65–90 ppm) is not clearly observed in all cases. However, peak intensity in the ^{13}C NMR does not quantify the corresponding functionality. While R-450 exhibits an allyl peak shoulder at 115–120 ppm, the corresponding peak of R-200 appears at a higher chemical shift, which indicates the presence of Cl in R-200.

Changes during this process are observed as variations in the particle size and cut surface morphology in the SEM images (Fig. 3). Dehydrochlorination radicals promote decomposition through the cleavage or modification of polymer chains, which leads to a reduction in the particle size. Backbone radical reactions at >450 °C cleave polymer chains and refine the residual structure. SEM images suggest that the polymer residues thermally degraded at 450 °C exist as smaller particles. The PVC solid residues prepared at temperatures below 350 °C undergo less deformation, and part of their initial structures remains, forming larger particle sizes and surface areas. SEM images of PVC and its thermally degraded residues reveal morphological differences during thermal treatment. Native PVC at room temperature exhibits a smooth, rounded granular morphology without defects or structural discontinuities. At 200 °C, the particles soften, which forms smoother surfaces and indicates the initial stage of melt-like deformations. At 250 °C, the softening degree increases, suggests a contraction or relaxation of internal stresses during thermal deformation. Structural changes appear at 300 °C, where sharp, plate-like fragments are formed. These features imply that the material transitions from a softened polymeric phase to a more brittle carbonaceous phase, which is attributed to PVC dehydrochlorination and structural rearrangements. At 350 °C, the residues present fracture surfaces with voids and microcracks, which indicates carbonization. At 450 °C, the surface becomes rough, and the melt-like characteristics observed at lower temperatures disappear.

Coupled with the observed decrease in the H/C and (H + Cl)/C ratios, these results indicate that most volatile compounds were eliminated, and a rigid, carbon-rich solid remained. Overall, the SEM analysis demonstrates the sequential transformation of PVC from softened and viscous structures at low temperatures to brittle and carbonized residues at elevated temperatures, which aligns with the thermal decomposition pathway of PVC.

Raman spectroscopy was conducted to investigate the evolution of the carbon bonding structure and the conjugation behaviour of the R-*X* materials (Fig. 4). The Raman spectra of R-200 and R-250 exhibit distinct peaks in the 1450–1500 cm^{-1} region, which correlate with the stretching modes of the conjugated C=C and C–C bonds along the polymer backbone. R-450 presents two important Raman peaks at 1595 cm^{-1} (G band) and 1364 cm^{-1} (D band). Based on these results, R-450 is characterized as a sp^2-hybridized carbon system. The G band corresponds to the

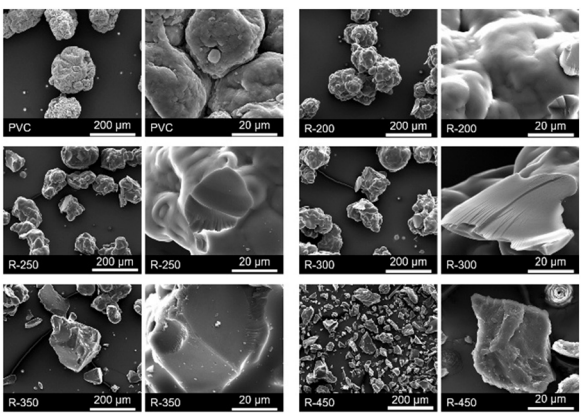

Fig. 3 SEM images of the PVC and R-*X* samples.

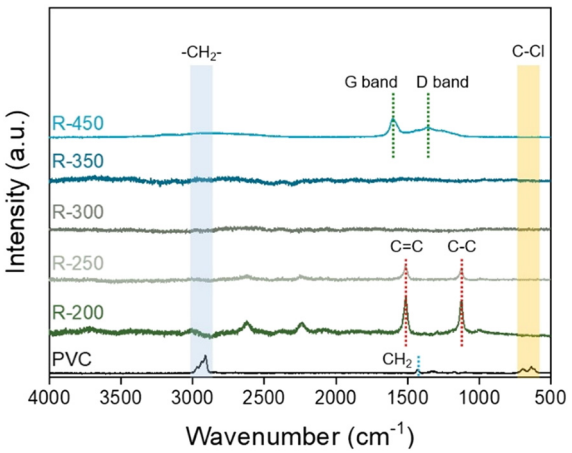

Fig. 4 Raman spectra of the PVC and R-*X* samples.

stretching vibration of the conjugated C=C bonds in sp^2 carbon domains, while the D band represents the aromatic rings activated by structural disorder. The appearance of the G and D bands suggests the formation of disordered yet conjugated sp^2 carbon frameworks during high-temperature treatments.

In the 2850–3000 cm^{-1} region, weak bands were appeared. These peaks correspond to aliphatic C–H stretching vibrations ($-CH_2-$), which decrease in intensity upon thermal treatment. Peaks at around 600–700 cm^{-1}, which correspond to C–Cl stretching vibrations, appear in samples containing residual PVC-derived compounds.

FT-IR spectroscopy was used to confirm the chemical functional groups and bonding environments of the samples, with emphasis on changes in the polymer and substituent groups (Fig. 5). The bands near 3037 cm^{-1} and 1600 cm^{-1} are assigned to aromatic =C–H stretching vibrations and aromatic ring C=C stretching vibrations, respectively; these peaks are sharp for R-450, which indicates the formation of aromatic structures. Bands in the 2850–2960 cm^{-1} range correspond to the aliphatic C–H stretching of $-CH_2-$ and $-CH_3$ groups, which are prominent in samples treated at lower temperatures. Bands in the 1400–1500 cm^{-1} region are assigned to $-CH_2-$ bending. Distinct bands observed in the 600–800 cm^{-1} region are assigned to C–Cl stretching vibrations, which are consistent with the presence of PVC-derived chloride compounds. As the reaction temperature increases, the overall intensities of the C–Cl and aliphatic C–H bands decrease. This indicates that the C–Cl bonds undergo cleavage at 250 °C through dehydrochlorination.

3.2 KOH treatment of thermally degraded PVC

The PVC solid residues generated *via* KOH treatment exhibit distinct tendencies in pore formation depending on the thermolysis temperature and activation steps (Fig. 6 and Table 2). The surface area of the PVC residue prepared at 350 °C was the largest. Activated carbon produced *via* a single-step reaction exhibits a larger surface area than that produced *via* a two-step reaction. When R-250, R-350, and R-450 are activated with KOH, the effects on their BET surface areas vary, reflecting differences in their chemical and physical structures. Because each reaction temperature produces distinct solid residues, the changes in the surface area after activation differ. KOH activation is selectively applied to R-250, R-350, and R-450. However, R-450 exhibits a significantly reduced efficiency. Therefore, detailed surface area analysis is performed on R-250 and R-350, where effective pore development is observed.

When PVC decomposes at 250 and 350 °C, polymer structures in the form of polyenes form. These structures possess unsaturated bonds, are amorphous and flexible, and yield solid residues with high reactivity toward KOH during activation. This reactivity leads to a higher BET surface area after KOH activation. Thus, polyene structures are favourable for pore formation. In contrast, at temperatures above 450 °C, polyene structures decompose and transform into more stable char forms. This char possesses a regular and dense structure, which reduces its reactivity with KOH. Consequently, pore formation during KOH activation is limited, and the increase in the BET surface area is minor.

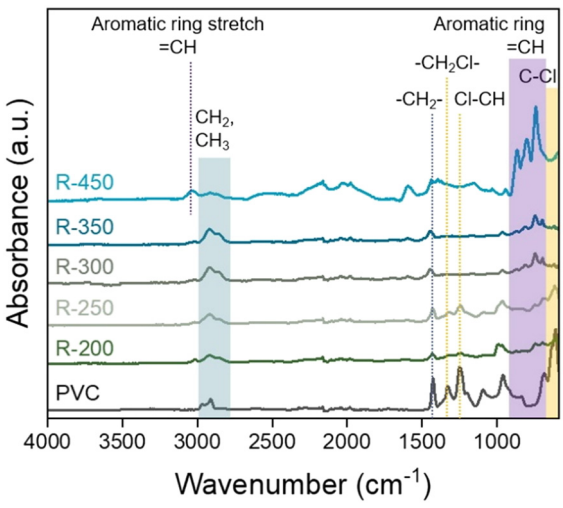

Fig. 5 FT-IR spectra of the PVC and R-*X* samples.

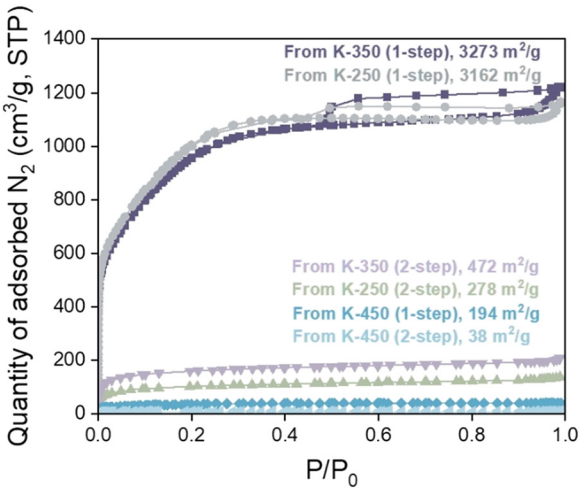

Fig. 6 N_2 physisorption results of the degraded PVC produced by one-step and two-step KOH treatment.

Table 2 Pore structures of the KOH-treated degraded PVC

Material	S_{BET} [a] ($m^2\ g^{-1}$)	$S_{micropore}$ [b] ($m^2\ g^{-1}$)
K-250 (1-step)	3162	3134
K-250 (2-step)	278	237
K-350 (1-step)	3273	3005
K-350 (2-step)	472	113
K-450 (1-step)	194	0.0001
K-450 (2-step)	38	0.00003

[a] BET surface area measured by BET model. [b] Micropore surface area measured by *t*-plot analysis.

Thus, the hard, dense char structure hinders KOH penetration into the pores.

PVC prepared at lower temperatures (250, 350 °C) yields a higher BET surface area after KOH activation. At these temperatures, amorphous and polyene structures provide favorable characteristics for activation and facilitate pore formation. In contrast, PVC prepared at high temperatures contains char, which suppresses the BET surface area increase. Previous studies emphasize the importance of amorphous structures and reactive bonds during the KOH activation process. Amorphous polymers lack crystalline structures; therefore, loosely bound intermolecular bonds facilitate KOH interactions and pore formation. This characteristic increases the BET surface area.

The two-step process, which involves heat treatment followed by KOH activation, yields a smaller BET surface area. Consequently, pore formation remains limited, which hinders the increase in surface area. In contrast, the one-step process, where thermal treatment and activation occurred simultaneously, enables efficient pore formation. These observations arise from the formation of an amorphous structure, which, upon treatment with KOH, generates pores and thereby increases the BET surface area. This approach avoids char pre-formation, which facilitates amorphous polymer activation and uniform pore formation. Heat treatment at 800 °C produces char, which possesses a stable, high-density structure that limits pore formation. These observations occurs because KOH does not etch the carbon effectively. Alternatively, PVC residues pyrolyzed at 450 °C form a dense, less active structure.

SEM analysis of the KOH-activated samples (K-250 and K-350) revealed morphological differences compared with thermally degraded PVC (Fig. 7). At the macroscopic scale (500 and 50 μm), both samples exhibited fragmented, granular structures. At higher magnifications (5 and 1 μm), the increased porosity that was generated by KOH activation became evident. This morphology indicates partial activation, where the reaction between KOH and the carbon matrix proceeds only to a limited extent.

HAADF-STEM images (Fig. 8) reveal finely distributed metal nanoparticles on various carbon supports for all samples. Bright contrast spots corresponding to metal species appear throughout the carbon matrix, while no large metal agglomerates or bulk-like particles are detected within the observed regions. Ru particles are anchored or partially embedded within the disordered carbon framework. The carbon supports display a heterogeneous and porous morphology, which contributes to the spatial confinement of the metal nanoparticles. Confined spaces and anchoring sites restrict the growth and aggregation of these metal nanoparticles.

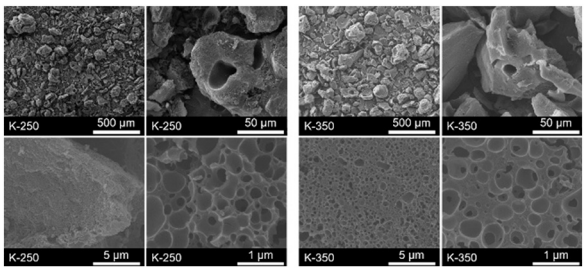

Fig. 7 SEM images of K-250 and K-350.

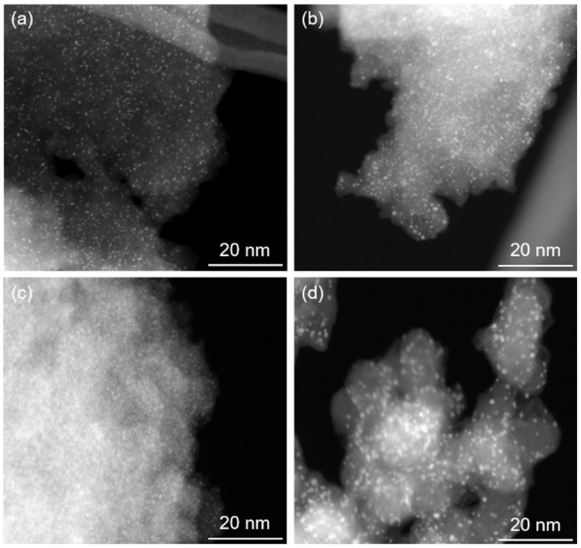

Fig. 8 HAADF-STEM images of Ru nanoparticles supported on (a) K-250, (b) K-350, (c) activated carbon, and (d) carbon black.

3.3 Hydrotreating of lignin-derived guaiacol using Ru supported on PVC-derived carbons

Guaiacol HDO reactions were conducted using Ru catalysts supported on various carbons (Fig. 9 and Table 3). Despite the relatively low H_2 pressure (10 bar), the complete conversion of guaiacol to products was achieved. GC-MS

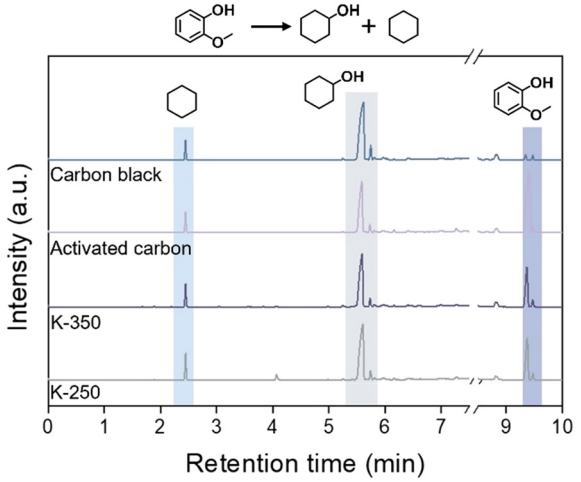

Fig. 9 GC-MS results of Ru catalysts supported on carbon black, activated carbon, K-350, and K-250.

Table 3 Reaction results using Ru supported on various carbons[a]

Support	Conversion of guaiacol (%)	Yield (%)	
		Cyclohexane	Cyclohexanol
Carbon black	~100	6.4	33.7
Activated carbon	92.3	7.2	27.4
K-350	92.3	6.9	25.2
K-250	73.9	6.9	23.7

[a] All catalysts contained 0.849–1.29 wt% of Ru, depending on the carbon support.

measurements (Fig. 9) and GC-FID measurements (Table 3) confirm that HDO-derived cyclohexane and cyclohexanol are the products over all catalysts. These observations indicate that the Ru catalysts supported on K-350 and K-250 exhibit higher catalytic activity than the catalysts supported on commercially available carbon materials.

For all catalysts, the combined yields of the major compounds, cyclohexane and cyclohexanol, are lower than the conversion of guaiacol. This difference in carbon balance occurs because of the formation of small cracked molecules, such as methane, and gas-phase light hydrocarbons. The formation of coke is also identified by TG analysis of all the spent catalysts, which exhibit thermal decomposition behaviour different from that of the corresponding fresh catalysts (Fig. S2 and S3). The lower yields of hydrodeoxygenated compounds are attributed to coke formation.

4. Conclusions

The upcycling of PVC wastes to a highly microporous carbon support *via* their thermal degradation followed by KOH treatment is proposed. While the PVC-derived solid prepared *via* thermal degradation at 450 °C exhibits neither high surface area nor porosity even after the KOH treatment, the solids degraded at 250–350 °C exhibit unusually high surface area and excellent microporosity. The highly microporous carbon support, prepared from PVC in this study, serves as a support for a hydrotreating catalyst (carbon-supported Ru), which exhibits good hydrotreating or hydrodeoxygenation activity compared with Ru supported on commercially available carbon supports. As PVC-derived carbons exhibit excellent pore structures, their applications extend to various fields.

Author contributions

Ju Young Kim: formal analysis (equal), investigation (equal), writing – original draft (equal). Seung Gun Kim: formal analysis (equal), investigation (equal), writing – original draft (equal). Jisong Kang: formal analysis (supporting), investigation (supporting). Jae-Wook Choi: methodology (supporting). Chun-Jae Yoo: funding acquisition (lead), project administration (lead), supervision (supporting). Chang Soo Kim: conceptualization (supporting), supervision (supporting), validation (supporting). Kyeongsu Kim: methodology (supporting), supervision (supporting), validation (supporting). Seongmin Jin: methodology (supporting), supervision (supporting), validation (supporting). Hyunjoo Lee: conceptualization (supporting). Kang Ho Song: methodology (supporting), supervision (equal). Jungkyu Choi: methodology (supporting), supervision (supporting). Dalsu Choi: conceptualization (equal), data curation (supporting), supervision (equal), writing – review and editing (equal). Jeong-Myeong Ha: conceptualization (equal), data curation (equal), supervision (equal), writing – review and editing (equal).

Conflicts of interest

There are no conflicts to declare.

Data availability

Supplementary information (SI): Fig. S1, Schematic depicting KOH activation processes of PVC residues; Fig. S2 and S3, TG and DTG results of catalysts. See DOI: https://doi.org/10.1039/d5cy01613d.

Acknowledgements

This work was supported by the Industrial Strategic Technology Development Program (RS-2024-00434298) funded by the Ministry of Trade, Industry and Resources (MOTIR), Republic of Korea. This research was also supported by the program of Development of Eco-friendly Chemicals as Alternative Raw Materials to Oil (2022M3J5A1085250) through the National Research Foundation (NRF) of Korea funded by the Ministry of Science and ICT, Republic of Korea.

Notes and references

1 X. Zhang, B. Gao, A. E. Creamer, C. Cao and Y. Li, *J. Hazard. Mater.*, 2017, **338**, 102–123.
2 N. Baig, I. Kammakakam and W. Falath, *Mater. Adv.*, 2021, **2**, 1821–1871.
3 S. Dutta, A. Bhaumik and K. C. W. Wu, *Energy Environ. Sci.*, 2014, **7**, 3574–3592.
4 I. Vollmer, M. J. F. Jenks, M. C. P. Roelands, R. J. White, T. van Harmelen, P. de Wild, G. P. van der Laan, F. Meirer, J. T. F. Keurentjes and B. M. Weckhuysen, *Angew. Chem., Int. Ed.*, 2020, **59**, 15402–15423.
5 M. H. Kudzin, D. Piwowarska, N. Festinger and J. J. Chruściel, *Materials*, 2023, **17**, 173.
6 L. Campisi, C. La Motta and D. Napierska, *Sci. Total Environ.*, 2025, **960**, 178276.
7 M. M. Shahsavar, N. Ghadami, M. Akrami, R. Aghlmand and M. Gheibi, *Annals of Environmental Science and Toxicology*, 2021, **5**, 099–0102.
8 I. Janajreh, M. Alshrah and S. Zamzam, *Sustain. Cities Soc.*, 2015, **18**, 13–20.

9 M. Sadat-Shojai and G.-R. Bakhshandeh, *Polym. Degrad. Stab.*, 2011, **96**, 404–415.
10 J.-W. Kim, C.-W. Park and J.-S. Kim, *Energy*, 2025, **334**, 137638.
11 W. Zhang, B. Yang, B. A. Jackson, J. Zhao, H. Shi, D. M. Camaioni, S. Kim, H. Wang, J. Szanyi, M.-S. Lee, J. G. Chen and J. A. Lercher, *Science*, 2025, **390**, 88–94.
12 J. Kang, J. Y. Kim, S. Sung, Y. Lee, S. Gu, J.-W. Choi, C.-J. Yoo, D. J. Suh, J. Choi and J.-M. Ha, *Environ. Pollut.*, 2024, **342**, 123074.
13 Y. Hu, M. Li, N. Zhou, H. Yuan, Q. Guo, L. Jiao and Z. Ma, *Sci. Total Environ.*, 2024, **908**, 168344.
14 Y. Wang, K. Wu, Q. Liu and H. Zhang, *Process Saf. Environ. Prot.*, 2021, **149**, 105–114.
15 M. Al-Yaari and I. Dubdub, *Polymer*, 2021, **13**, 4359.
16 S. H. Gebre, M. G. Sendeku and M. Bahri, *ChemistryOpen*, 2021, **10**, 1202–1226.
17 I. Yang, M. Jung, M.-S. Kim, D. Choi and J. C. Jung, *J. Mater. Chem. A*, 2021, **9**, 9815–9825.
18 H. Yu, J. Qu, Y. Liu, H. Yun, X. Li, C. Zhou, Y. Jin, C. Zhang, J. Dai and X. Bi, *Sci. Total Environ.*, 2022, **806**, 150903.
19 K. Anshu and S. K. Thengane, *Biomass Convers. Biorefin.*, 2025, **15**, 11751–11775.
20 F. Yang, X. Liu, M. Li, C. Uguna, W. Wang and C. Sun, *Renewable Sustainable Energy Rev.*, 2023, **180**, 113279.
21 O. K. Choi, E. H. Song and H. Kim, *Sci. Total Environ.*, 2024, **947**, 174599.
22 P. Zhao, T. Li, W. Yan and L. Yuan, *Environ. Technol.*, 2018, **39**, 977–985.
23 M. Ling, D. Ma, X. Hu, Z. Liu, D. Wang and Q. Feng, *Chemosphere*, 2023, **316**, 137718.
24 X. Li, Y. Chen and X. Guo, *Process Saf. Environ. Prot.*, 2024, **183**, 945–951.
25 N. Miskolczi, L. Bartha and A. Angyal, *Energy Fuels*, 2009, **23**, 2743–2749.
26 A. López, I. De Marco, B. Caballero, M. Laresgoiti, A. Adrados and A. Aranzabal, *Appl. Catal., B*, 2011, **104**, 211–219.
27 J. Sun, T. Ding, X. Zhao, P. Wang, W. Chen and J. Yu, *Waste Disposal Sustainable Energy*, 2025, 1–12.
28 Y. Kwak, J. Eom, H. Nam and C. Nam, *Chemosphere*, 2024, **359**, 142283.
29 N. Yao, X. Wang, Z. Yang, P. Zhao and X. Meng, *J. Hazard. Mater.*, 2023, **456**, 131687.